 doi:10.20944/preprints201811.0534.v1

Article

Saint Venant and Navier-Stokes models for tsunami simulations

Camille Journeau[1], Kévin Pons[2,3], Richard Marcer[4]*

[1] Principia; camille.journeau@principia.fr
[2] Principia; kevin.pons@principia.fr
[3] Université de Toulon, IMATH; kevin.pons@univ-tln.fr
[4] Principia; richard.marcer@principia.fr
* Correspondence: richard.marcer@principia.fr; Tel.: +33-044-298-1640

Abstract: Into the frame of the French TANDEM project (Tsunamis in the Atlantic and the English ChaNnel: Definition of the Effects through numerical Modelling) Principia has been working on the development and qualification of two in-house CFD software's: the 2D EOLE-SV (Saint Venant) model for simulation of large scale tsunami propagation from the source up to coastal scale and the 3D EOLE-NS (Navier-Stokes) model dedicated to tsunami coastal impact modelling. This paper presents a large range of test cases carried out into the frame of the project and dedicated to the validation of numerical codes in various tsunami wave conditions. The main aspects of phenomena such as wave generation, propagation and coastal impact are investigated on academic situations. A real case simulation is concerned as well, the devastating 2011 Tohoku event which is compared with in-situ data.

Keywords: tsunami; CFD; Saint Venant (SV) model; Adaptive Mesh Refinement (AMR); large scale propagation; 3D Navier-Stokes (NS) model; coastal impact.

1. Introduction

This work has been performed in Principia within the framework of the French TANDEM project (Tsunamis in the Atlantic and the English ChaNnel: Definition of Effects through numerical Modelling) which is dedicated to the appraisal of coastal effects due to tsunami waves on the French coastlines. TANDEM aims at drawing lessons from the 2011 catastrophic tsunami in Japan. It allows designing, adapting and checking numerical methods of tsunami hazard assessment to define, as accurately as possible, the tsunami hazard for the French Atlantic coastlines in order to provide guidance for risk assessment on coastal civil and nuclear facilities.

To reach these objectives, qualification of numerical codes has been set up, addressing the various stages of a tsunami event: generation, propagation, run-up and inundation. Principia have been working on the validation of two complementary models: a depth-averaged Saint Venant model developed by Principia and Université de Toulon [1] for large scale tsunami propagation simulation, and a fully 3D Navier-Stokes model developed by Principia especially for complex wave breaking and coastal impact problems [2], [3].

An overview of the results obtained with both codes aiming at being applicable to tsunami modelling, is presented. The validation process has been done on several academic test cases having experimental data for comparisons, and a real tsunami event:

- Breaking of a solitary wave on a constant slope [4].
- Propagation of a solitary wave on a 2D reef [5], [6].
- Russel's wave generator (vertical block falling down a water volume at the rest) [7], [8].
- Tsunami generation due to a 3D wedge sliding down a slope [9].

Preprints (www.preprints.org) | NOT PEER-REVIEWED | Posted: 22 November 2018 doi:10.20944/preprints201811.0534.v1

- Tsunami impact on an urban area [10].
- Tohuku tsunami in 2011.

2. Description of CFD codes used

2.1. EOLE-NS (Navier-Stokes)

The EOLE-NS code developed by Principia since 1990 is a multi-phase URANS model which solves the two-phase Navier-Stokes equations on structured curvilinear multi-blocks meshes, possibly moving or deforming. It is based on a pseudo-compressibility technique using a dual time stepping method and a second order finite volume scheme for spatial discretization [2]. The interface motion between the different phases is simulated from an implicit VOF model which avoids any CFL constraint and therefore allows globally large time steps. The interface displacement, which corresponds to the transport of the VOF function, may be ensured by a classical Eulerian equation or by an improved Eulerian-Lagrangian method developed by Principia, especially for complex wave breaking problems [2], [3]. A six degrees of freedom mechanical solver is integrated in the code allowing the modelling of fluid / structure coupling.

The multi-phase NS model is particularly well adapted for complex flow simulations.

2.2. EOLE-SV (Saint-Venant)

The 2D EOLE-SV code is developed jointly at Université de Toulon and Principia. It contains, among others, the Saint Venant model based on the very long wave assumption leading to non-dispersive depth averaged equations. The solver is based on a finite volume method and unstructured meshes. It uses the robust Godunov solver with a second order MUSCL scheme in space and a Runge Kutta integration in time.

An adaptive mesh refinement (AMR) method based on blocks cutting is implemented (Figure 1). It enables mesh refinement only where significant phenomena append, allowing optimization of CPU time computation. Details of the methodology are given in [11].

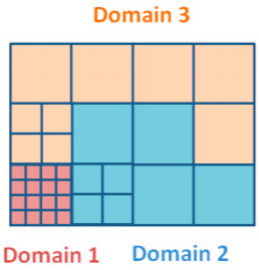

Figure 1. Example of non-structured and non-conforming AMR mesh distributed on 3 domains.

The Saint Venant model (often called NLSW for Non Linear Shallow Water) is well-adapted to simulate large scale tsunami propagation when horizontal processes are preponderant. But when the tsunami approaches the coast, very complex physics phenomena may occur such as wave breaking and interaction with coastal structures, or strong bathymetry gradients. Then 3D modelling is required to get more accurate results.

3. Model validation on tsunami test cases

Preprints (www.preprints.org) | NOT PEER-REVIEWED | Posted: 22 November 2018 doi:10.20944/preprints201811.0534.v1

3.1. Breaking of a tsunami wave on a constant slope

The experiment, schematically described on Figure 2, has been carried out at the California Institute of Technology [4]. A wave maker allows the generation of a solitary wave propagating at first on a constant channel depth area and then on a constant slope beach. The common parameters of this test case are given on Figure 2. The available experimental data concern the interface evolution of the plunging wave breaking at different times.

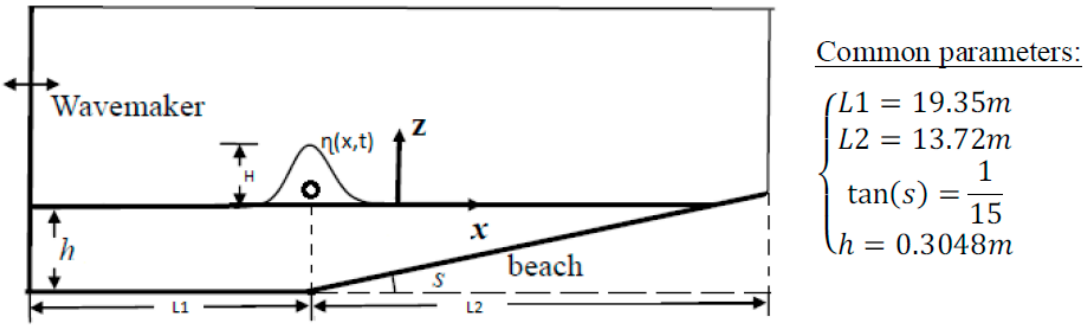

Figure 2. Experimental device - Breaking of a tsunami wave on a constant slope.

The test case is simulated with the NS code. The wave is initialized with a 1st order Boussinesq solitary wave solution with η the wave amplitude equal to 0.45h. Figure 3 gives comparisons with experiments of the wave interface at two different instants of the breaking process. Results are on the whole satisfactory as the NS model allows capturing with a good phasing and topology the complex physics of the plunging process characterized by a rapid and large deformation of the interface. It can be noticed that a refinement of the mesh would likely improve the representation of the plunging wave crest sharpening. Figure 4 displays an example of the NS model capability with a plunging wave simulation of splash-up and bubble entrainment processes.

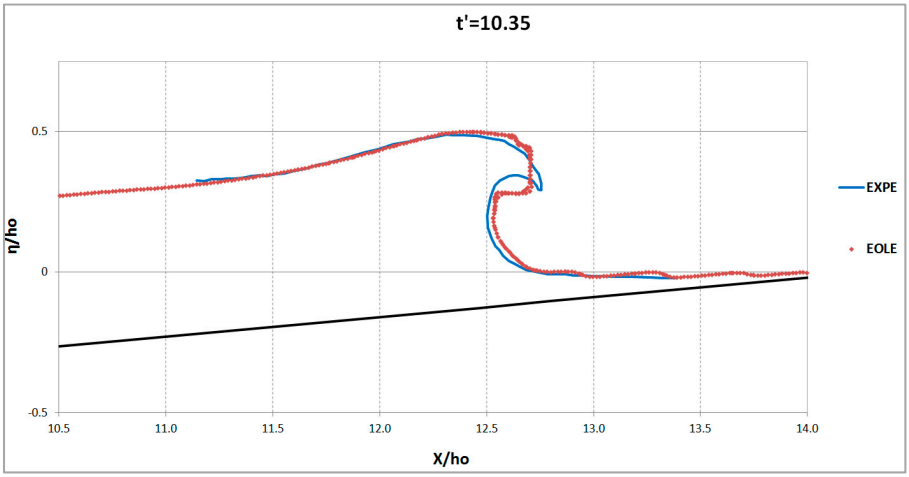

Preprints (www.preprints.org) | NOT PEER-REVIEWED | Posted: 22 November 2018 doi:10.20944/preprints201811.0534.v1

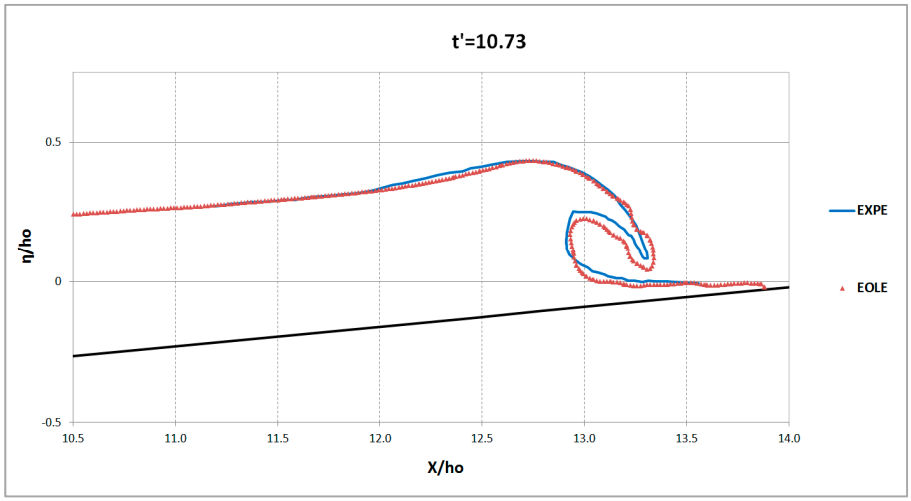

Figure 3. Wave shape comparison at different times (with $t' = t\sqrt{g/h_0}$ and $h_0 = 0.3048\ m$ - NS model (red dots), experiments (blue line).

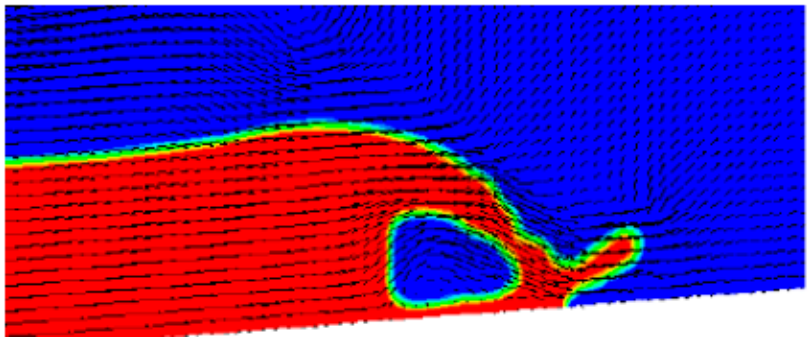

Figure 4. Simulation of wave breaking with the NS code.

3.2. Solitary wave reflecting on a 2D vertical reef

This study is based on a set of experiments carried out at the O.H. Hinsdale Wave Research Laboratory [5, 6]. They involve the propagation, run-up, overtopping and reflection of high amplitude solitary waves on two-dimensional reefs. Their purposes are on one hand to investigate the processes relative to breaking, bore formation, dispersion and transition from sub to super-critical flows while, on the other hand, providing data for the validation of near-shore wave models in fringing reef.

The geometry of the experiment is showed on Figure 5. The basin is 104m long. The reef starts at x = 25.9m, with a nominal slope of 1/12. The actual slope is such that the height of 2.36m is reached after 28.25m. At this station, a 0.2m height crest is mounted. Regarding boundary conditions, reflective walls at both ends of the domain (x = 0m and x = 83.7m) are used. The 0.75m input solitary wave gives a dimensionless wave height η/h = 0.3 since the initial depth at still water is 2.5m. To simplify boundary conditions, the solitary wave is initially placed at x = 17.6m which in reality is where the experimental data places the peak at the dimensionless time $t' = t\sqrt{g/h_0}$ = 47.11. Numerical wave gauges are placed at the exact same position as the experimental ones (Figure 5).

Preprints (www.preprints.org) | NOT PEER-REVIEWED | Posted: 22 November 2018 doi:10.20944/preprints201811.0534.v1

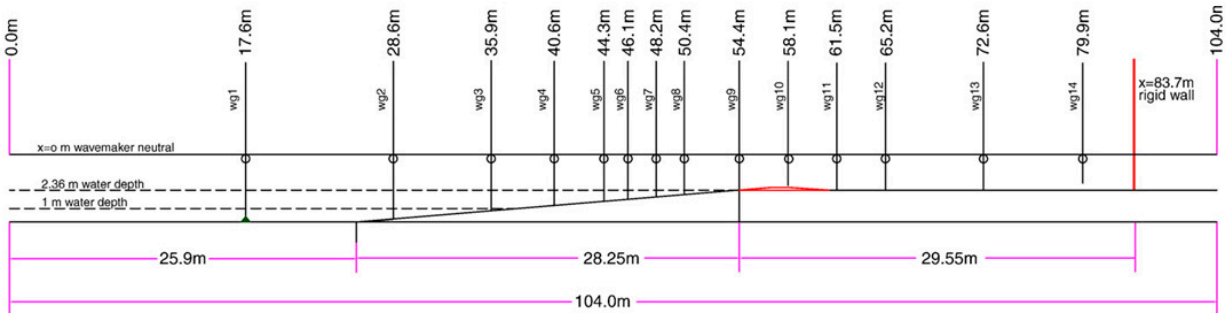

Figure 5. Channel and 2D reef geometry (in red).

The initial depth at still water (h_0 = 2.5m) gives a partially submerged reef crest. Results are available for the NS model. Comparisons with the experimental data of water level distribution along the flume at dimensionless times $t' = t\sqrt{g/h_0}$ are given on Figure 6. For clarity's sake, only snapshots representative of propagation, breaking and overtopping phases have been selected.

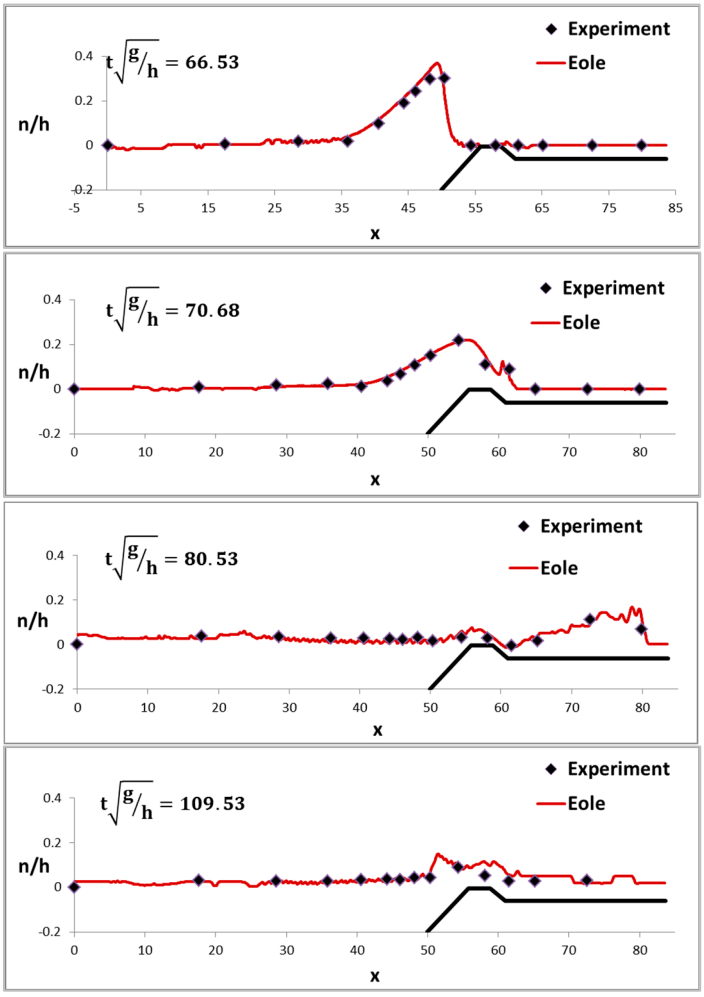

Figure 6. Water level at t'=66.53, t'=70.68 and t'=109.53.

The first graph, at t'=66.53, shows the propagation and shoaling of the solitary wave. The NS model provides a peakier wave with regards to the experiments but the code is on the whole satisfactory with the data. At t'=70.68 the waves overtops the reef, begins to break and initializes the bore formation. Then the sharp bore moves upstream (t'=80.53) and reflects on the right wall. The resulting reflecting wave passes above the reef for a second time, forming a second bore which

Preprints (www.preprints.org) | NOT PEER-REVIEWED | Posted: 22 November 2018 doi:10.20944/preprints201811.0534.v1

propagates upstream (t'=109.53). On the whole, the model provides precise front positions and amplitudes of the wave during the different phases of the wave propagation.

Figure 7 compares the computed and recorded surface elevation time series at three specific wave gauges, two upstream of the reef in the sloping area and one downstream the reef on the constant depth zone. The first peak of the recorded data at the upstream WG2 and WG8 gauges show the initial propagation of the wave (WG2) and the moment just before breaking (WG8). For both gauges the later peaks highlight the dispersive and reflective waves induced by the reef. The downstream WG13 gauge is representative of the propagation of the initial and reflected bores.

The hydraulic jump developed at the fore reef produces a train of waves over the increasing water depth and the resulting undulations are intensified as higher harmonics are released. The NS model provides a good description of the early phase of the process and a satisfying prediction of undular bore even though higher frequency oscillations are missing in the results.

Detailed comparisons of this Navier-Stokes simulation with results obtained from different codes (NS, NLSW and dispersive depth integrated models) are available in [12].

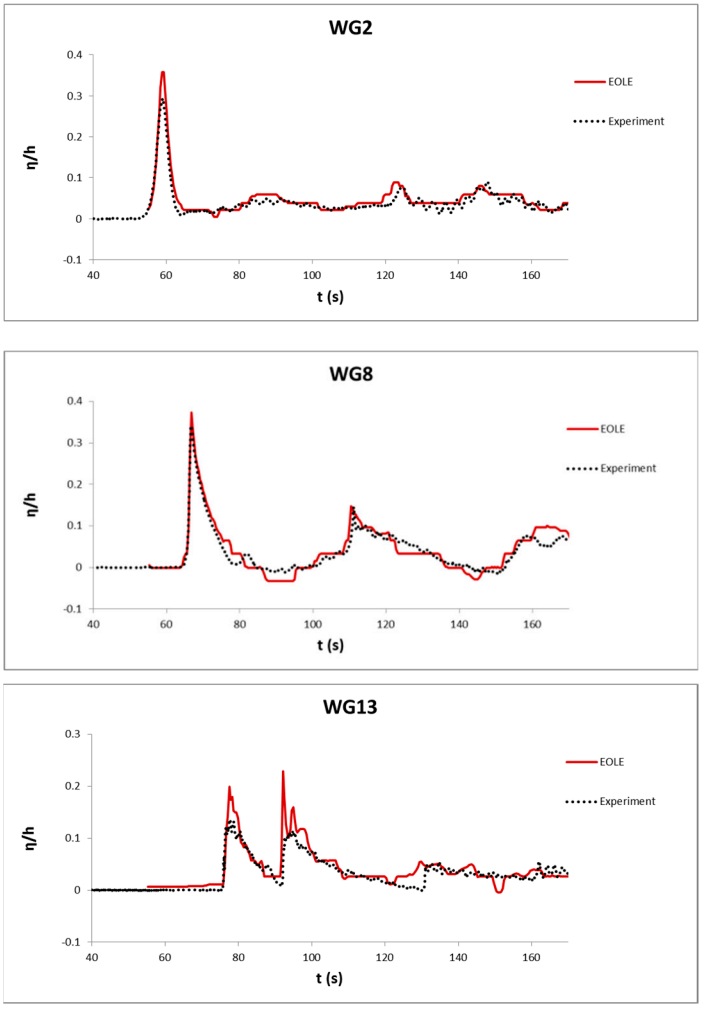

Figure 7. Time series in WG2 (propagation), WG8 (breaking), and WG13 (bore propagation).

3.4. Russel's wave generator

Preprints (www.preprints.org) | NOT PEER-REVIEWED | Posted: 22 November 2018 doi:10.20944/preprints201811.0534.v1

This case concerns the generation of a long wave induced by the vertical fall of a rectangular rigid body and its interaction with the underlying water. It is based on the experiment published in [7] and [8]. The purpose here is to check the accuracy of the NS model in a case of strong interactions between a rigid body and the free surface. In terms of engineering relevance, this case involves the main physics of massive cliffs or ice bodies falling into water and is therefore representative of some tsunami generation processes. Figure 8 represents a sketch of the experiment which was carried out in a 9meters long flume with a water depth D.

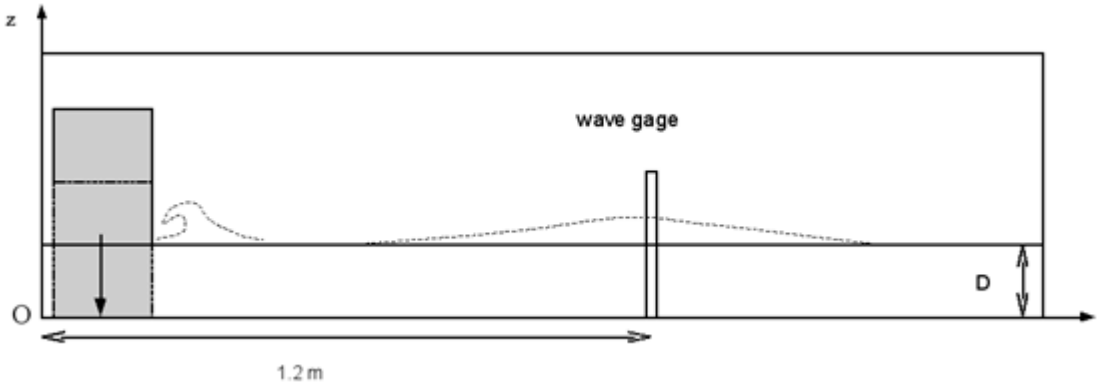

Figure 8. Russel's wave generator: sketch of the experimental device.

At t=0s, a 38.2kg rectangular block placed just above still water level is released. Experiments are repeated for several water depths, D=0.288m, D=0.210m and D=0.116m. In each case, the block's vertical position and the free surface elevation is measured as a function of time at a wave gage located at 1.2m from the leftward extremity of the flume. Values of H and B (Figure 9) are also estimated from videos post processing.

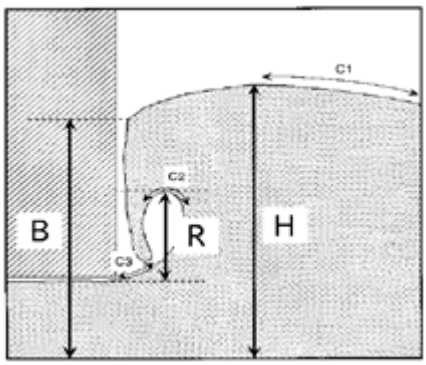

Figure 9. Russel's wave generator: definition of B and H.

To solve fluid/solid interactions, the NS model calculates the resulting pressure force on the block and deduces the free motion from Newton's law. Figure 10 presents a snapshot of the simulation highlighting the formation of the wave due to the block falling down.

Preprints (www.preprints.org) | NOT PEER-REVIEWED | Posted: 22 November 2018 doi:10.20944/preprints201811.0534.v1

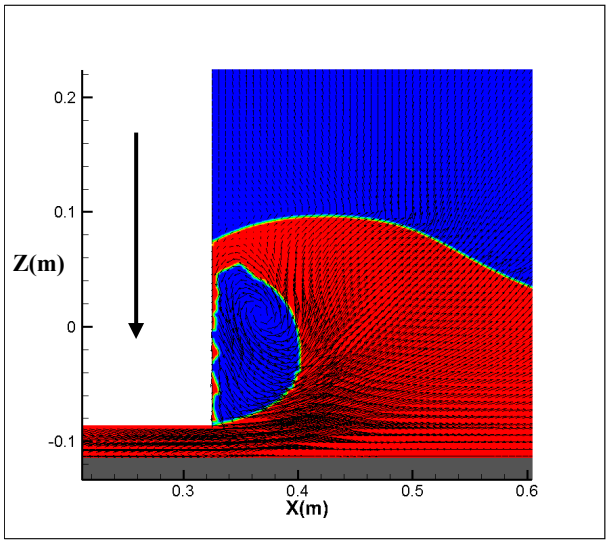

Figure 10. Snapshot of simulation for D=0.288m

Table 1 summarizes the wave height monitored at a distance of 1.2m from the leftward extremity of the flume (see Figure 8), for various initial water depths. On the whole numerical estimations show a very good accuracy except for the smaller water depth for which the amplitude is slightly underestimated. Table 2 lists values of H and B (defined in Figure 9) for D=0.210m and confirms the ability of the model to correctly reproduce the complex shape of the wave interface as the block is moving down.

Table 1. Wave height at x=1.2m for various water depths

	D(m)		
	0.116	**0.210**	**0.288**
Experiment	0.109	0.092	0.093
NS model	0.093	0.094	0.098
Error (%}	15	2	5

Table 2. Values of H and B for an initial depth of D=0.210m

	H(m)	**B(m)**
Experiment	0.333±0.01	0.303±0.02
NS model	0.317	0.296
Error (%}	5	2

Figure 11 displays a comparison of the free fall solid motion, between NS results and experiments. The curve is to be read from right to left with increasing time. Z/D≈1 and Z/D→0 correspond respectively to the extreme positions of the block during the process: release and bottom approach. Very satisfactory results are obtained for the fluid / solid coupling model with especially an accurate maximum velocity brought out at the same depth than experiments. Increasing velocity just after the release and decreasing velocity as the block approaches the bottom are correctly reproduced as well.

Preprints (www.preprints.org) | NOT PEER-REVIEWED | Posted: 22 November 2018 doi:10.20944/preprints201811.0534.v1

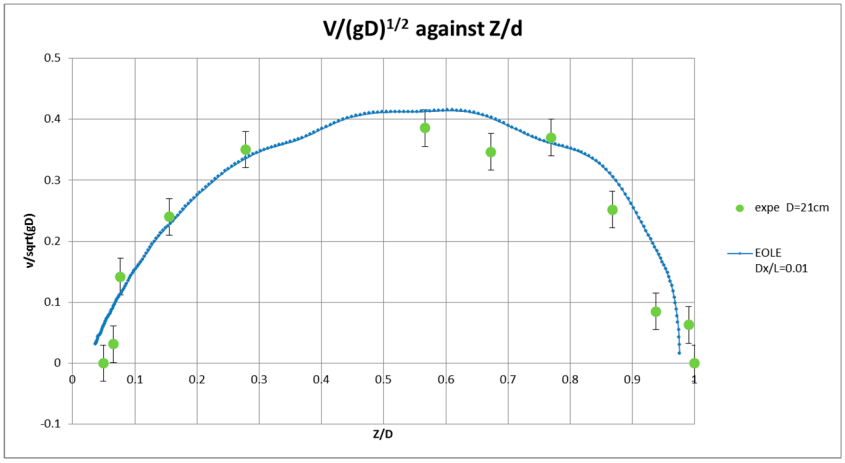

Figure 11. Solid velocity versus solid vertical position – D=0.21m.

3.5. Tsunami generation due to a 3D wedge sliding down a slope

This test-case performed with the NS code concerns the modelling of a tsunami generated by a submarine landslide which is represented in the experimental device [9] by a wedge sliding down a 1:2 plane beach slope. Dimensions of the test bench are given on Figure 12. Comparisons are done with measurements from laboratory data published [9] where different initial wedge positions regarding the free surface height were tested: wedge partially emerged and fully immersed. When the wedge is partially emerged, the top is located at Δ=0.1m above the free surface; when it is fully immerged, the top is located at Δ=-0.025m below the free surface. Wave elevation is monitored at different gauges (wave gauges 1 and 2) whereas the wave run-up is extracted from data on three "runup" gauges which measure the vertical height (positive or negative) reached by the wave around its initial level (=0). The detailed positions of the gauges are given in Figure 12**.**

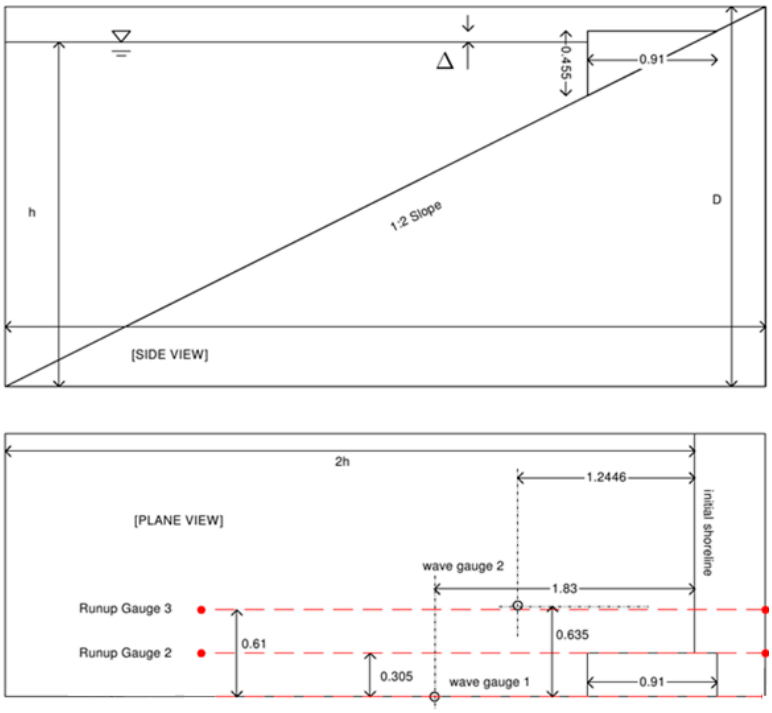

Figure 12. Sketch and dimensions of the test bench, here for the partially emerged case (Δ=0.1m) – side view and top view (half of the geometry).

Preprints (www.preprints.org) | NOT PEER-REVIEWED | Posted: 22 November 2018 doi:10.20944/preprints201811.0534.v1

In the simulation, the wedge is fully immersed at initial time with a depth of 2.5mm (distance from the free surface to the top of the wedge) and at rest. Then the block is moved downward along the slope according to a recorded law of motion issued from experiments, with a maximum velocity of 0.22 m/s.

Figure 13 shows visualizations of the wave induced by the sinking of the solid. Red and blue colours express respectively the positive and negative elevations of the wave around level 0. Successive wave crests and troughs are visible and the corresponding fluctuations of wave elevations (with maximum amplitudes ≈ [-10cm, +5cm]), and run up are highlighted on the different gauges (Figure 14). Wave gauges show that the first trough and crest are correctly reproduced as well as the wavelength of the waves, except a delay on the third crest for the gauge 2. Amplitudes of run-up are on the whole satisfactorily reproduced, especially when considering the small values of the fluctuations to capture in this problem (less than 5cm).

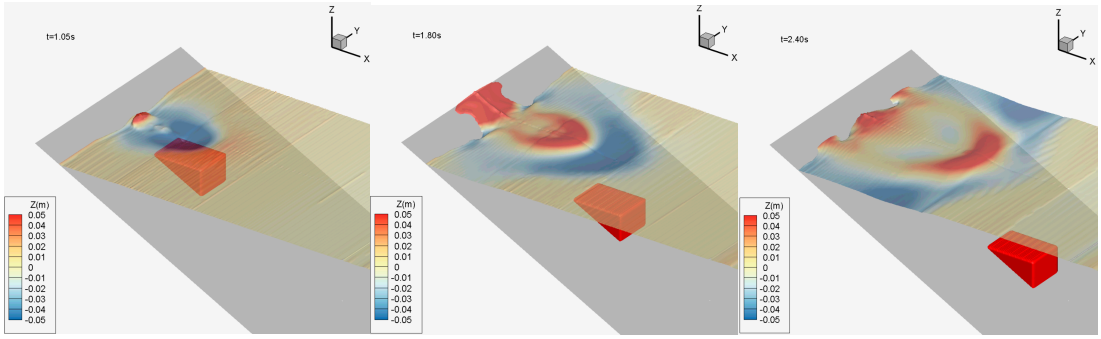

Figure 13. Wave propagation and run-up due to sliding wedge motion (t=1.05s, t=1.8s and t=2.4s from left to right). Fully immerged case (Δ=-0.025m).

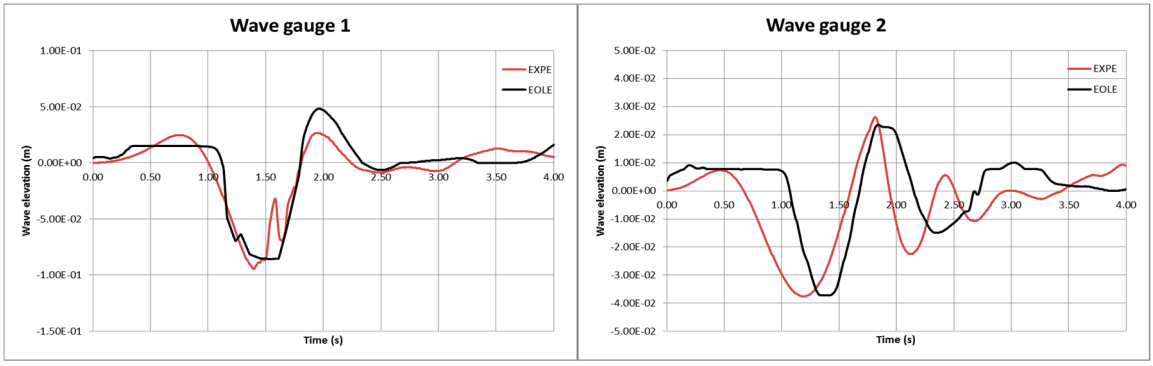

Figure 14. Comparison of wave elevations on gauge 1 and gauge 2 (blue symbols on Figure 12).

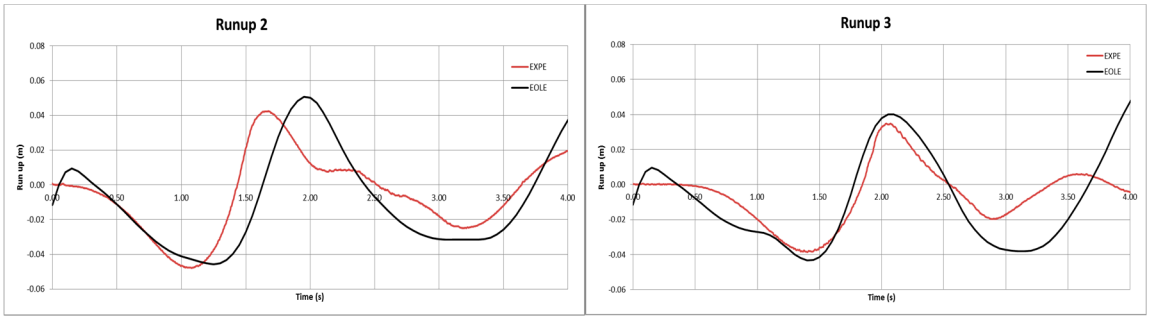

Figure 15. Comparison of wave run-up on gauges runup 2 and runup 3 (red symbols on Figure 12).

Preprints (www.preprints.org) | NOT PEER-REVIEWED | Posted: 22 November 2018 doi:10.20944/preprints201811.0534.v1

3.5. Seaside experiment: impact on a urban area

This experimental case has been carried out in the Oregon State University basin [10]. A complex topography was built including a seawall and several buildings inspired by the city Seaside, Oregon. The offshore wave (height 0.2m and period 10s) was designed to correspond to the estimated tsunami wave height for "500 years" Cascadia Subduction Zone tsunami. This test case is particularly interesting to bring out the ability of a CFD model to simulate flows on complex topography including many "macro roughnesses". An overview of the experimental set-up and the probes disposition in the city is shown on Figure 16.

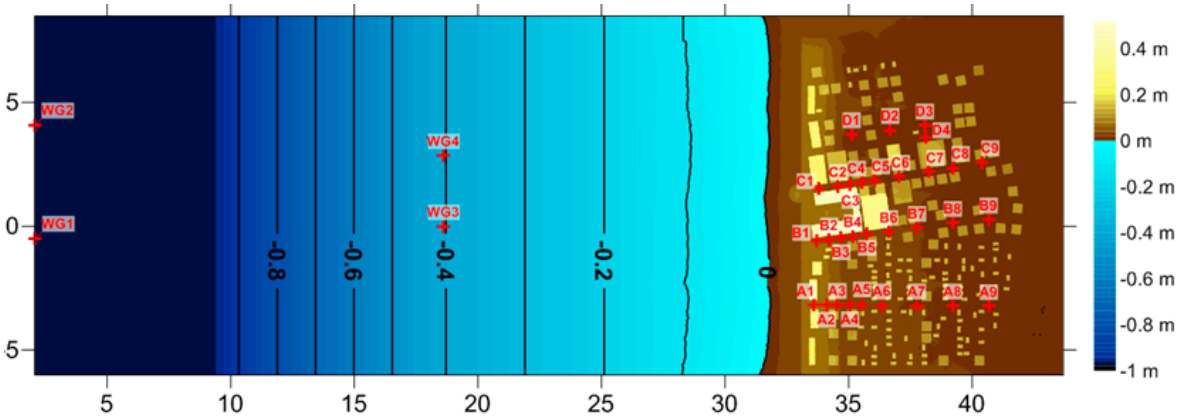

Figure 16. Sensors locations.

The simulation is carried out with the NS model on a multi-block mesh of 9 million cells illustrated in the Figure 17. The wave generated experimentally by a piston-type wave maker is numerically represented by a 1st order Boussinesq solitary wave. All the boundaries are supposed to be walls.

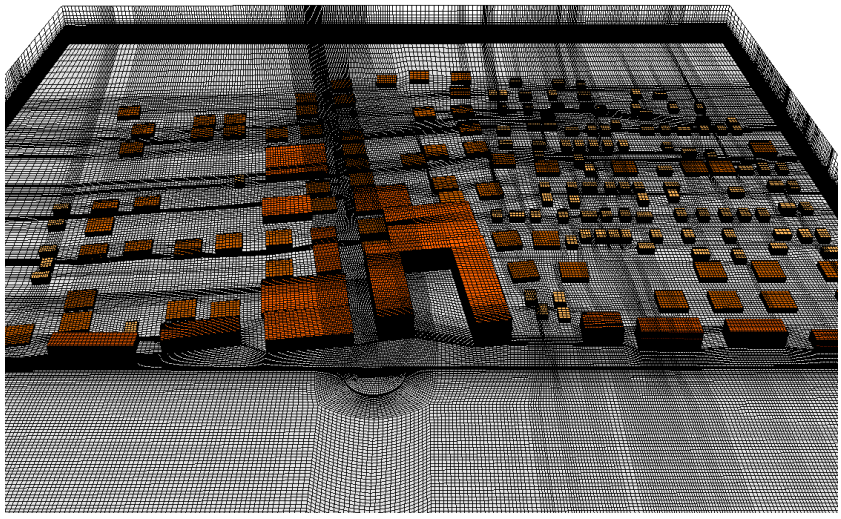

Figure 17. Multi-block structured mesh of the city for the NS model.

Figure 18 shows snapshots of the tsunami impact against the buildings of the city. For numerical results red and blue colors express respectively the positive wave propagation velocity (Umax≈1ms/s) and the reflecting wave velocity (Umin≈-0.5ms/s) around the rest (in white).

Preprints (www.preprints.org) | NOT PEER-REVIEWED | Posted: 22 November 2018 doi:10.20944/preprints201811.0534.v1

Comparisons with measurements are done at two different instants of the flooding process. Very good results can be noticed for the flooding according to the layout of the city, as well as the reflecting wave by the buildings.

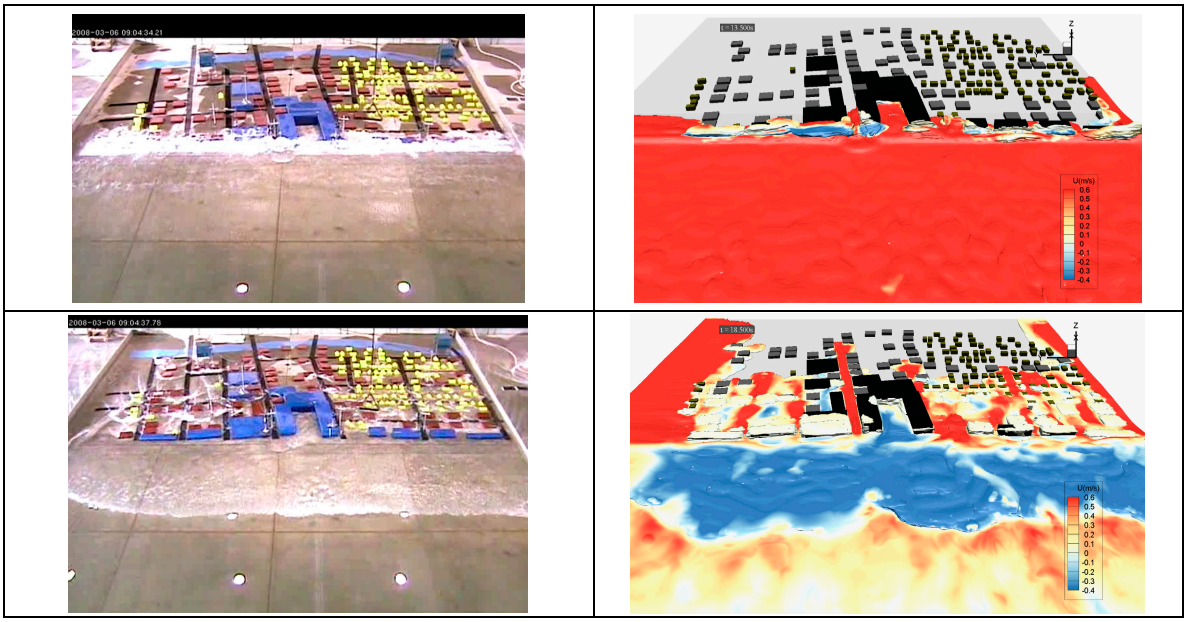

Figure 18. Comparisons of the wave field at two instant.

Figure 19 shows comparisons of the free surface elevation time series. For readability reason only a sample of gauges is analysed: near the shore-line at the wave impact (B1), in the middle of the city (B6) and in the rear of the urban area (B9). The behaviour of wave elevations on gauges Ai, Ci and Di are very similar to the gauges Bi presented here.

On the whole numerical results of elevation are very satisfactory both in amplitude and phasing, whatever the position of the probes. Large amplitude peaks are observed at the impact on the shore-line whereas the wave height decreases strongly as it propagates inside the city. Even for the further inland area (B9 probe) for which the run-up amplitude is expected to be the weaker (maximal amplitude of only ~5 cm), the numerical model allows to capture the very small wave elevation amplitudes.

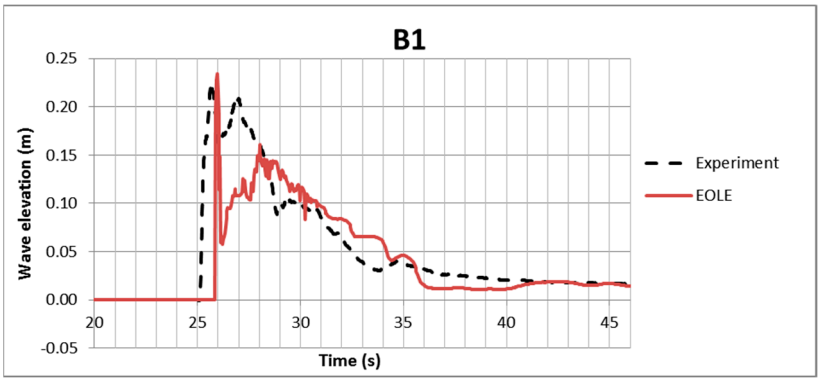

Preprints (www.preprints.org) | NOT PEER-REVIEWED | Posted: 22 November 2018 doi:10.20944/preprints201811.0534.v1

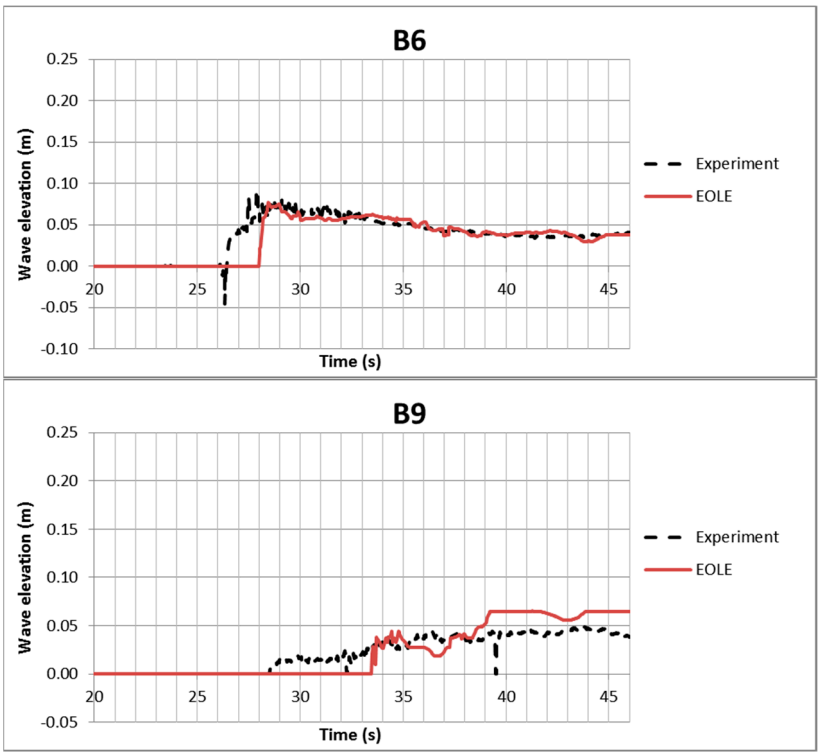

Figure 19. Time series of free surface elevation at 3 gauges. From top to bottom B1, B6, B9.

Figure 20 displays cross-shore velocity time series on the same positions as previous probes elevations. Velocities are globally well predicted for the peak values and the time profiles. A quick decrease of the flow velocity is brought out near the shore line (B1) whereas inside the city (B6) the current dynamic is longer maintained due to local ducting effects. It can be noticed that the model tends to underestimate the flow dynamic on the furthest inland area (B9) where the wave amplitude is very small (~5 cm). This is probably due to a lack of vertical mesh refinement in this very remote area.

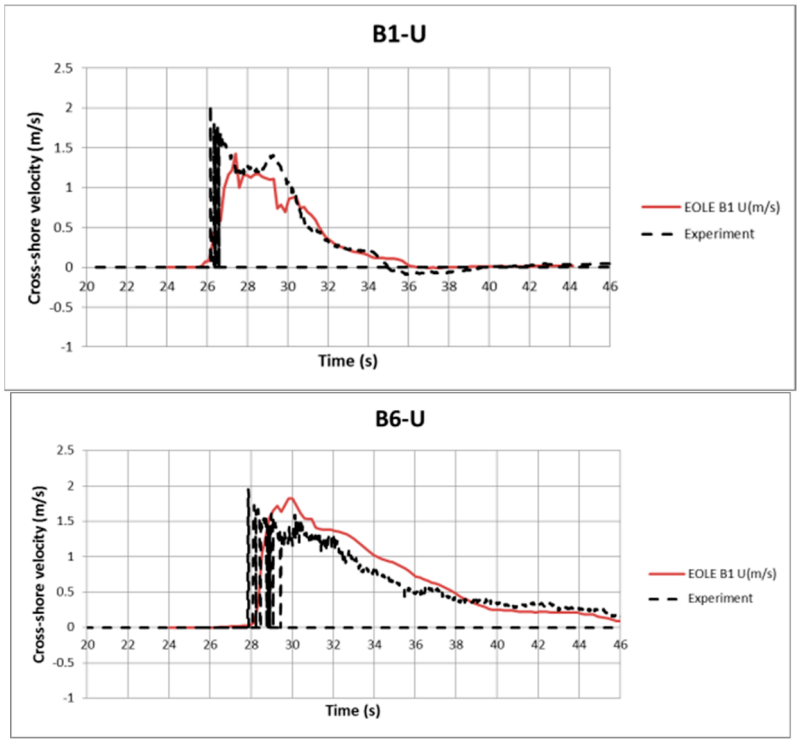

Preprints (www.preprints.org) | NOT PEER-REVIEWED | Posted: 22 November 2018 doi:10.20944/preprints201811.0534.v1

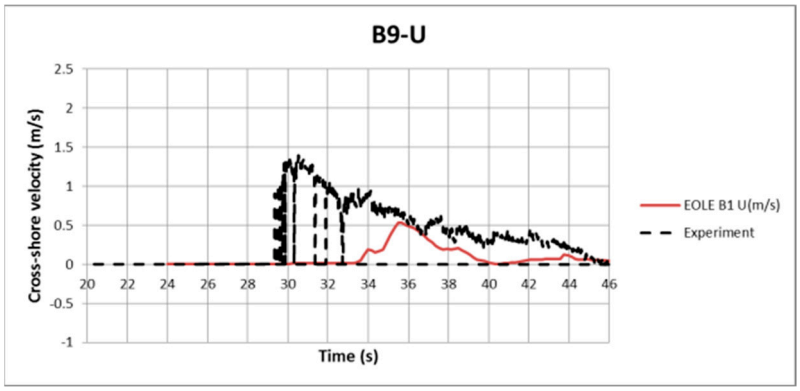

Figure 20. Time series velocity at three gauges. From top to bottom: B1, B6 and B9.

Benchmarks and comparisons of this NS simulation with results obtained with different NSLW Boussinesq codes are available in [13]. On the same test case, different technics for building modelling in the NS code are presented in [14].

4. Simulation of the 2011 Tohuku tsunami event

The 2011 earthquake of magnitude 9.1 in Tohoku-Oki (Japan) triggered a tsunami among the most devastating. It broke a lot of seawalls and breakwaters of the Japan coastline, which were designed for smaller critical events. The Tohuku-Oki tsunami has been studied by many authors and reproduced with different numerical models such as [15], [16], [17] and [18]. Simulation is here carried out with the SV code using the AMR (Adaptive Mesh Refinement) method. The model covers a large area around Japan in order to assess the reliability of the code for long wave's simulation over very large scales.

The 2011 Tohoku-Oki event is exceptionally well documented. Actually, water buoys and seismic sensors close to the epicentre are available along with water level data on buoys in far field and quite close to the coastline. Therefore, it is possible to qualify the ability of the numerical model to account for the large scale propagation from the source as well as typical physical processes occurring in coastal area such like shoaling, refraction and diffraction, due to bathymetry / topography gradients.

The tsunami source is taken from [19] and considers a slip source alone. The slip distribution is divided into 55 sub faults. Static sea bottom deformation is calculated by a rectangular fault model assuming an elastic half-space [20]. Horizontal displacement effects are also taken into account.

The model covers an area of about 2500km x 5000km. The bathymetry discretization provides an accuracy in the range of [10m-600m], respectively in the coastal and far field areas. The mesh refinement permitted by the AMR method is 10m in the coastal zone allowing the modelling of local breakwater impacts, and up to 4800 m in the far field. Bathymetry and mesh discretization are shown on Figure 21 with ``nc'' the local mesh size range given by the AMR method and ``nb'' the bathymetry interpolation accuracy during the mesh adaptation. In fact, a constraint has been introduced in the AMR method to locally adjust the zone refinement. This method enables the concentration of computational resources on areas of interest such as coastal bays.

Preprints (www.preprints.org) | NOT PEER-REVIEWED | Posted: 22 November 2018 doi:10.20944/preprints201811.0534.v1

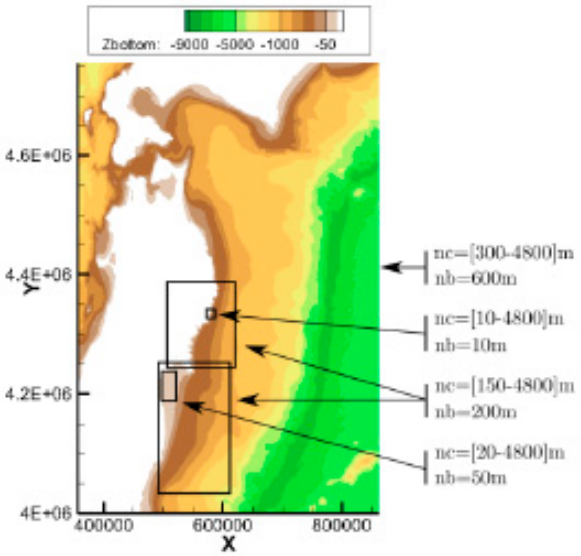

Figure 21. Bathymetry and grid levels depending on the different areas. The most important refinement is concentrated in the Kamaishi bay (nc $\geq 10m$).

Figure 22 yields a global view of the tsunami propagation within the first two hours. The first wave hits the Japan coast before 30min after the earthquake. As the Pacific Ocean deepness is large (about 5000m) far off the Japan coasts the transoceanic propagation is very quick, about 800km/h.

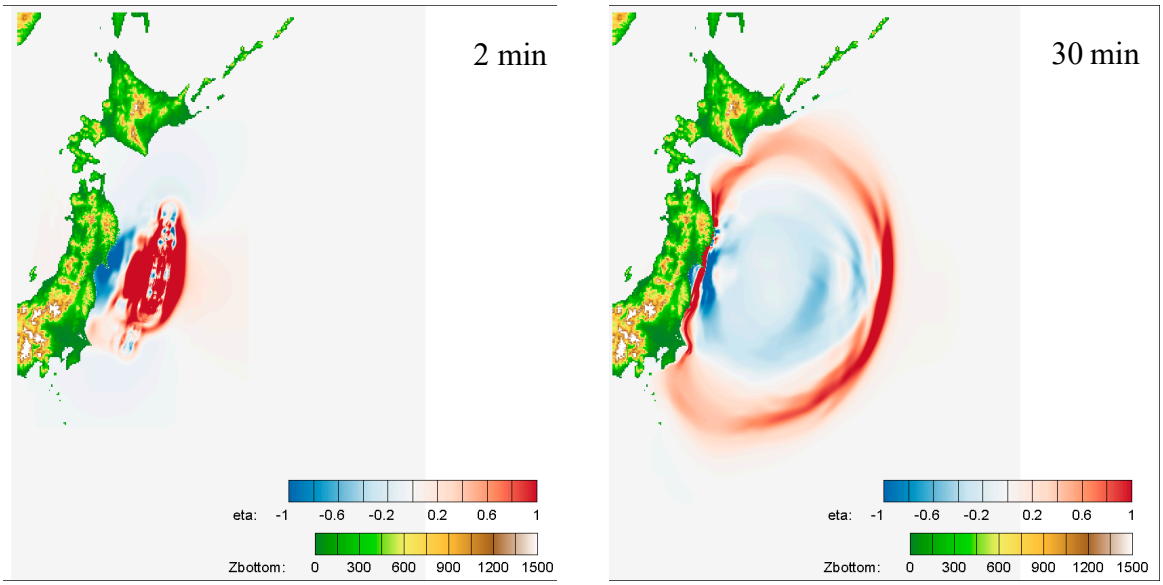

Preprints (www.preprints.org) | NOT PEER-REVIEWED | Posted: 22 November 2018 doi:10.20944/preprints201811.0534.v1

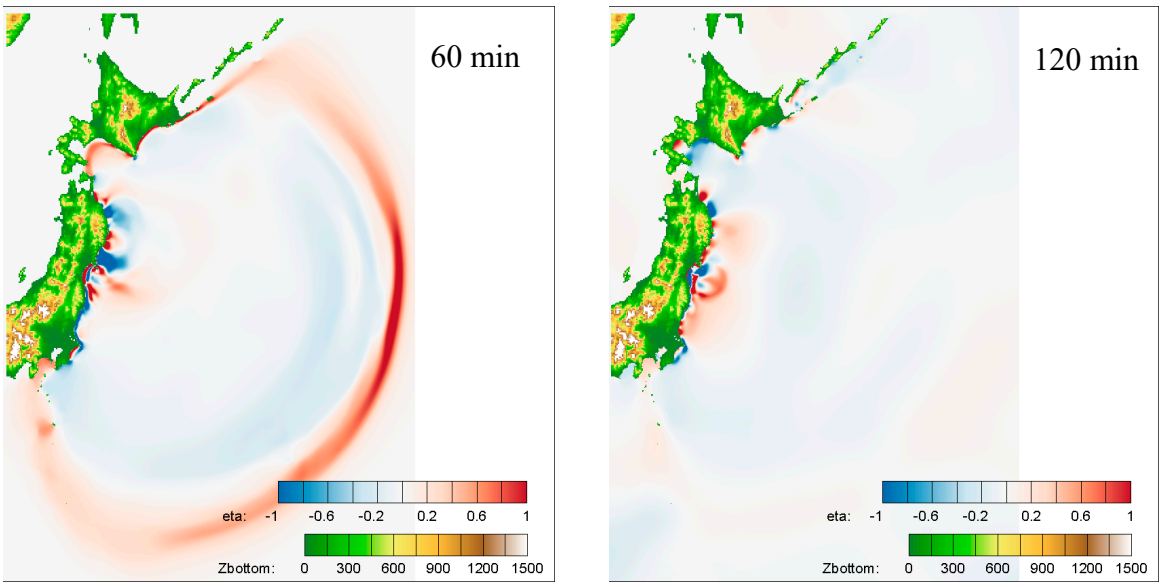

Figure 22. Tsunami propagation – global view. Note that the free surface color scale is chosen to highlight the large scale propagation but the leading wave is much higher than 1m amplitude when approaching the coast.

Two kinds of quantitative wave elevation comparisons have been performed with far field DART buoys and with GPS buoys closer to the coast (Figure 23).

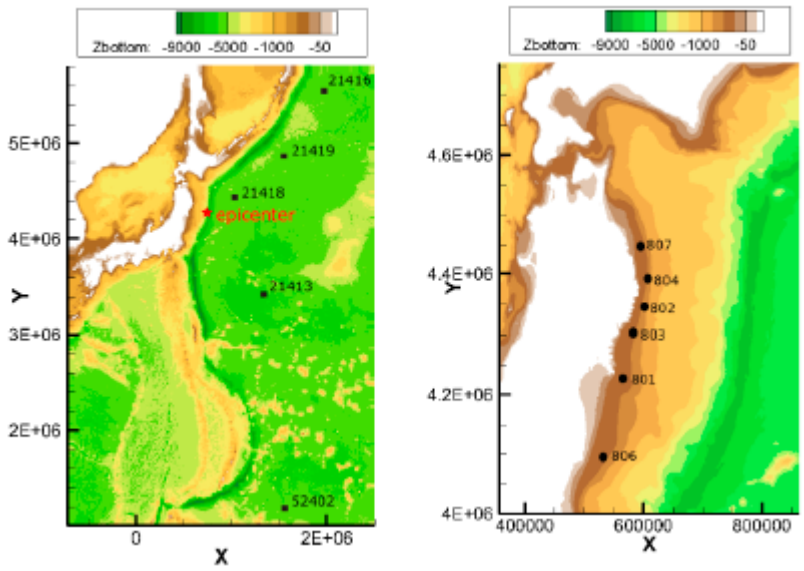

Figure 23. Positions of the far field DART buoys (left) and the nearshore GPS (right).

Figure 24 presents far-field wave elevation results compared to DART buoys data. Numerical results are very comparable to in-situ data especially close to the epicentre (buoy 21418) with correct amplitude and phasing. Elevations are slightly underestimated far away from the source (buoys 21413 and 21419), probably due to a lack of mesh refinement in this far field area or dispersive effects. But it must be noticed that these two buoys bring out quite small wave amplitudes.

Preprints (www.preprints.org) | NOT PEER-REVIEWED | Posted: 22 November 2018 doi:10.20944/preprints201811.0534.v1

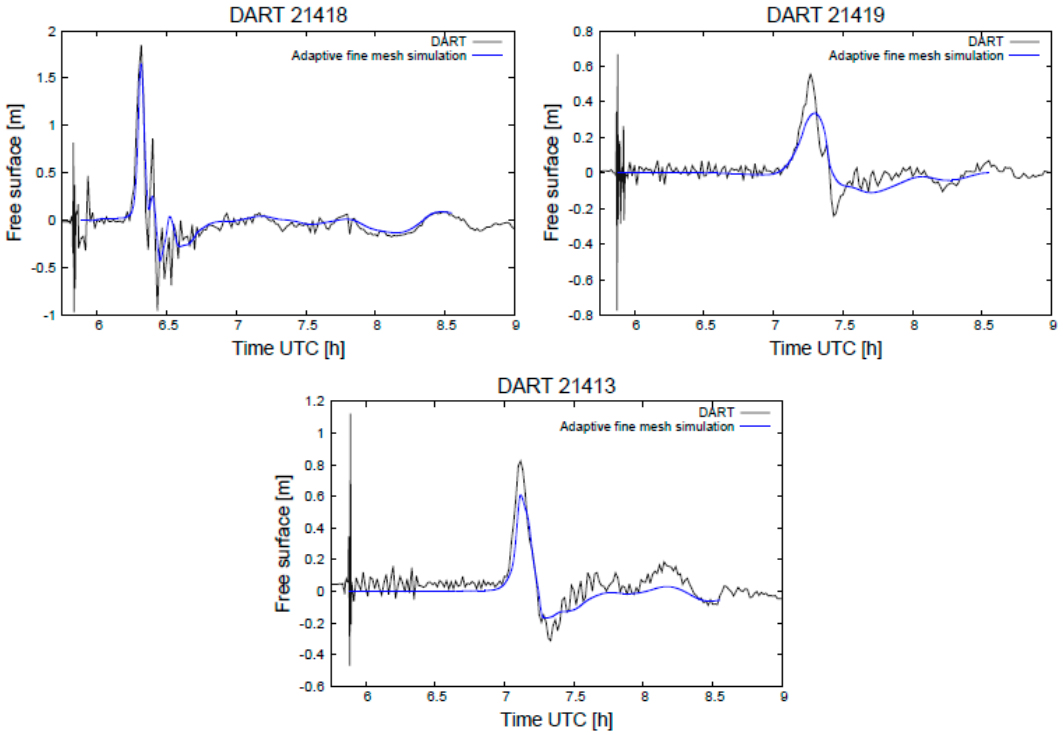

Figure 24. Comparisons of the SV model with DART data.

Numerical results for nearshore GBS buoys are on the whole very satisfactory (Figure 25), and better than the preliminary results obtained with the same code based on simplified hypotheses, especially about the source model [18]. Therefore, wave amplitudes and phases are well represented for all buoys, except for the farthest buoy from the source (GPS 806) where a slight underestimation of the wave amplitude is observed. As the amplitude shift appears right at the beginning of the simulation it may highlight a weakness of the tsunami source model used in the simulation.

Preprints (www.preprints.org) | NOT PEER-REVIEWED | Posted: 22 November 2018 doi:10.20944/preprints201811.0534.v1

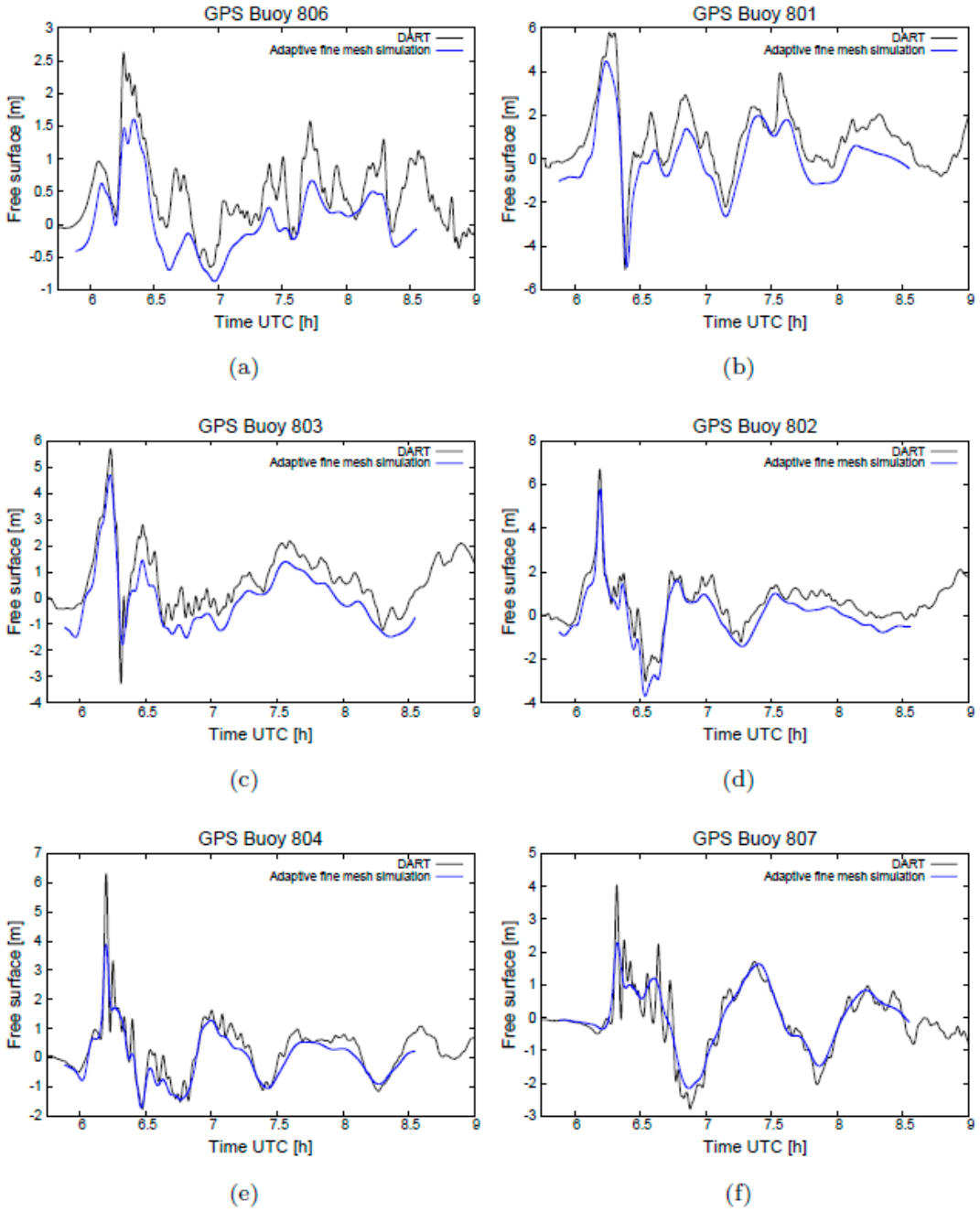

Figure 25. Comparisons of the SV model with GPS data.

A zoom of the tsunami impact in the Kamaishi Bay is concerned. During the event, the breakwaters located at the entry of the bay partially collapsed (Figure 26**Error! Reference source not found.** and Figure 27**Error! Reference source not found.**).

To highlight the impact of the breakwaters regarding the bay protection, two configurations have been studied. The first case considers the breakwaters as keeping their integrity whereas in the second case they are supposed collapsed. In this last case, as it was impossible to find a detailed description of the damaged breakwaters after the event and then the position of the different elements which have toppled and slipped, it is considered that the breakwaters have instantaneously collapsed on their entire length. The geometrical detail of the removed elements considered in the simulation is given in Figure 28. The bathymetry cut off has been done at the foot

Preprints (www.preprints.org) | NOT PEER-REVIEWED | Posted: 22 November 2018 doi:10.20944/preprints201811.0534.v1

of the breakwaters at the level of -23.5m. Note that even without breakwaters, the shallow depth of the foot will still have a slight effect on the wave propagation (shoaling, diffraction).

Figure 26. Picture of Kamaishi Bay with partially collapsed breakwaters extracted from [21].

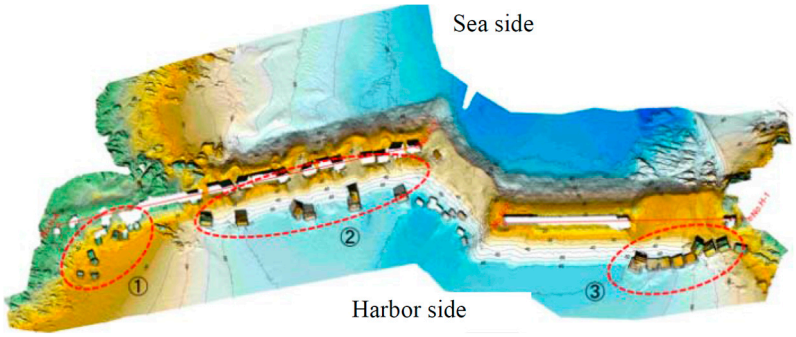

Figure 27. Sketch of the damaged breakwaters extracted from [21].

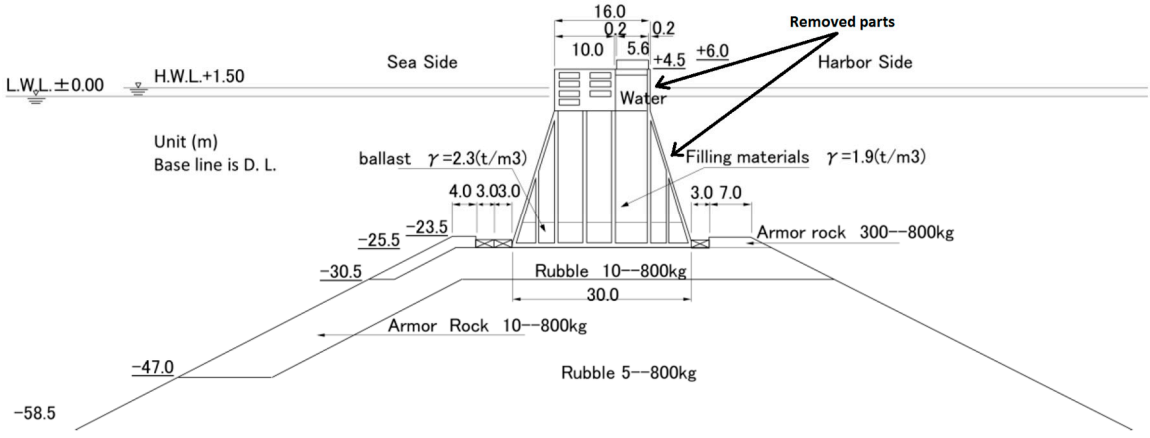

Figure 28. Sketch of the breakwaters extracted from [21] with removed parts detail (down to -23.5 m depth) used for the simulation "without breakwaters".

Preprints (www.preprints.org) | NOT PEER-REVIEWED | Posted: 22 November 2018 doi:10.20944/preprints201811.0534.v1

The tsunami propagation in Kamaishi Bay during flooding with and without the breakwaters is shown on Figure 29. In both cases, large amplitudes of the wave are observed (more than 10m) leading to a significant flooding of the coastal land. However, the breakwaters clearly limit the wave run-up. As the breakwaters have partially been damaged during the wave entry, the reality might be estimated by considering these two scenarios envelope.

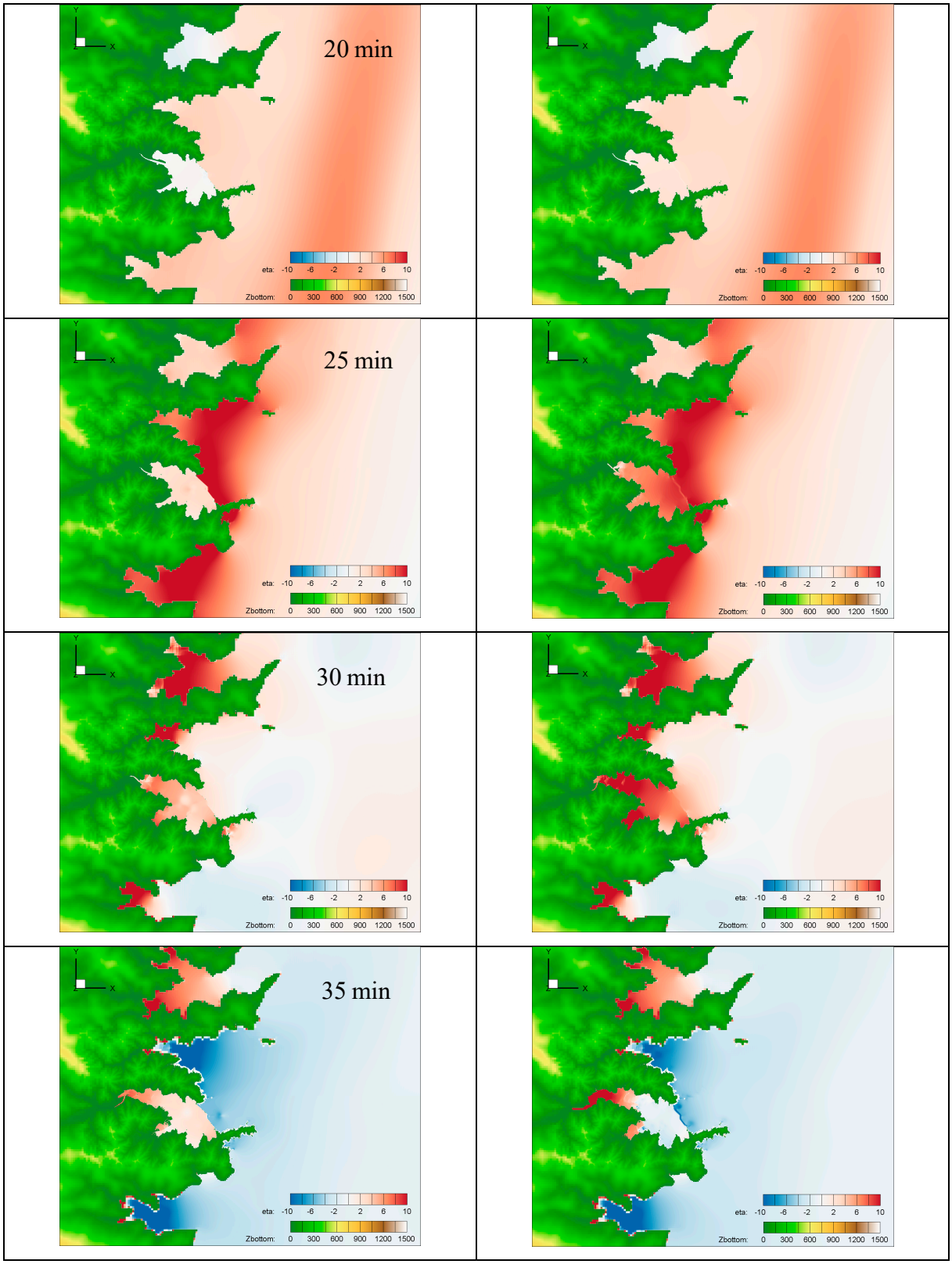

Figure 29. Tsunami propagation in Kamaishi bay during 15 min of flooding with breakwaters (left pictures) and without (right pictures).

6. Conclusion

Following the objectives of the TANDEM project Principia have been working on the validation of its in-house 2D SV and 3D NS codes for tsunami simulations. A qualification protocol has been built mainly from validations on well-documented academic and experimental test cases, each one dedicated to analyze specific tsunami physics (propagation, breaking, impact, run-up,…), as well as a real event. This step-by-step validation approach allowed evaluating the performances of the 2D and 3D models regarding the overall complex physics.

The NS model rather adapted for 3D coastal tsunami impact modelling is able to represent with a good accuracy most of the complex coastal processes such as wave breaking, hydraulic bore formation on irregular sea bottom and wave/building interactions. Moreover this model allows the reproduction of the wave generation due to landslide or falling rock, from a dynamic fluid / structure coupling.

The 2D SV model is very performing for large scale tsunami propagation simulation. The study of the Tohuku tsunami shows that this code is also capable to give interesting results at coastal scale, like for instance the influence of breakwaters regarding their protection against the wave and the issued run-up.

Acknowledgment:

The authors want to thanks Rodrigo Pedreros, Sylvestre Le Roy and Anne Lemoine from BRGM for providing the source model of the Tohuku tsunami.

This study has been performed within the Work Package 1 (Benchmarking of numerical methods) of the TANDEM project (Tsunamis in the Atlantic and the English ChaNnel: Definition of the Effects through numerical Modelling) (2014–2018), with partial funding from the PIA-ANR program (Programme Investissements d'Avenir, Agence Nationale de la Recherche) from the French Government under grant 2013-RSNR-01.

Author Contributions: Richard Marcer a Senior CFD expert, Camille Journeau a CFD engineer, Kévin Pons a PhD student in Principia and the Institut de Mathématiques de l'Université de Toulon.

References

1. Pons, K.; Golay, F.; Marcer, R. Adaptive mesh refinement method applied to shallow water model: a mass conservative projection, Topical problems of fluid mechanics 2017**.**
2. Guignard, S.; Marcer, R.; Rey, V.; Kharif, C.; Fraunié, P. Solitary wave breaking on sloping beaches: 2D two phase flow numerical simulation by SL-VOF method. *Eur. J. Mech. B, Fluids* **2001**, *20*, pp.57-74.
3. Biausser, B.; Guignard, S.; Marcer, R.; Fraunié, P. 3-D two phase flows numerical simulations by SL-VOF method, *Int. J. Numer. Meth. Fluids* **2004**, 45:581-604.
4. Li Y.; Raichlen F. Breaking criterion and characteristics for solitary waves on slopes, *J. Waterway, Port, Coast. Ocean Engng*. **1998**, Vol 124(6), pp.329-333.
5. Roeber, V. Boussinesq-type model for nearshore wave processes in fringing reef environment, PhD Thesis, University of Hawaii, 2010.
6. Roeber, V.; Cheung, K.F. Boussinesq-type model for energetic breaking waves in fringing reef environments, *Coast. Eng*. **2012**, 70:1–20.
7. Monaghan, J.J.; Kos, A.; Scott Russell's wave generator, *Phys. Fluids* **2000**, 12(3):622–630.
8. Russel J. Report on waves, *Rep. Brit. Assoc. for the Advancement of Science* **1844**, 311–390.
9. Liu, P.L.F.; Wu T.R.; Raichlen, F.; Synolakis, C.E.; Borrero, J.C. Runup and rundown generated by three-dimensional sliding masses. *J. Fluid Mech.* **2005**, Vol. 536, pp 107–144.
10. Park H.; Cox D.T.; Lynett P.J.; Wiebe D.M.; Shing S. Tsunami inundation modelling in constructed environments: a physical and numerical comparison to free surface elevation, velocity and momentum flux, *Coastal Engineering* **2013**, 79:9-21.
11. Golay, F.; Ersoy, M.; Yuschenko, L.; Sous, D. Block-based adaptive mesh refinement scheme using numerical density of entropy production for three-dimensional two-fluid flows. *International Journal of Computational Fluid Dynamics*, **2015**, Vol. 29(1), pp 67–81.
12. Kazolea M.; Filippini A.; Ricchiuto M.; Abadie S.; Martin Medina, M.; Morichon, D.; Journeau, C.; Marcer, R.; Pons, K.; LeRoy, S.; Pedreros, R.; Rousseau, M. Wave propagation, breaking, and overtopping on a 2D reef: a comparative evaluation of numerical codes for tsunami modelling, *European Journal of Mechanics – B/Fluids* **2017**. https://doi.org/10.1016/j.euromechflu.2017.10.010.
13. Violeau, D.; Ata, R., Benoit, M.; Joly, A.; Abadie S.; Clous, L.; Martin Medina, M.; Morichon, D.; Chicheportiche, J.; Le Gal, M.; Gailler, A.; Hébert, H.; Imbert, D.; Kazolea M.; Ricchiuto M.; LeRoy, S.; Pedreros, R.; Rousseau, M.; Pons, K.; Marcer, R.; Journeau, C.; Silva Jacinto, R. A database of validation cases for tsunami numerical modelling, 4th IAHR Europe Congress – Sustainable hydraulics in the area of global change 2016, Liege Belgium.
14. Audiffren C.; Forgues V.; Marcer R. CFD simulation of a tsunami impacting a coastal city including numerous buildings, *Advances in Hydroinformatics. Springer Water. Springer, Singapore*, **2018**, pp 629-639.
15. Popinet, S. Adaptive modelling of long-distance wave propagation and fine-scale flooding during the Tohoku tsunami, *Natural Hazards and Earth System Sciences* **2012**, 12(4):1213–1227.
16. Grilli, S. T.; Harris, J. C.; Bakhsh, T. S. T.; Masterlark, T. L.; Kyriakopoulos, C.; Kirby, J. T.; Shi, F. Numerical Simulation of the 2011 Tohoku Tsunami Based on a New Transient FEM Co-seismic Source: Comparison to Far- and Near-Field Observations, *Pure Appl. Geophys. 170*, **2013**, 1333–1359.
17. Kirby, J.T.; Shi, F.; Tehranirad, B.; Harris, J.C.; Grilli, S.T. Dispersive tsunami waves in the ocean : Model equations and sensitivity to dispersion and coriolis effects, *Ocean Modelling*, **2013**, 62 :39–55.
18. Pons, K.; Marcer, R.; Golay, F. The Saint-Venant model for tsunami propagation simulation: Application to the 2011 Tohoku event, 2016, XIVèmes Journées Nationales Génie Côtier – Génie Civil, Paralia.
19. Sakate K.; Fujii Y.; Harada T.; Namegaya Y. Time and space distribution of coseismic slip of the 2011 Tohoku earthquake as inferred from tsunami wave form data. Bulletin of the Seismological Society of America 2013, Vol. 10(2B), pp.1473-1492.
20. Okada, Y. Surface deformation dee to shear and tensile faults in a half-space. Bulletin of the Seismological Society of America, 1985, Vol. 75(4), pp 1135-1154.
21. Arikawa, Taro, et al. "Failure mechanism of Kamaishi breakwaters due to the Great East Japan earthquake tsunami." Coastal engineering proceedings, 2012, Vol. 1(33).